Advanced Nano Research
Volume 6, Issue 1, pp. 29-43, 2023
DOI: https://doi.org/10.21467/anr.6.1.29-43

ISSN: 2581-5164

RESEARCH ARTICLE

Fabrication Method of Carbon-based Materials in CH_4/N_2 Plasma by RF-PECVD and Annealing Treatment for Laser Diodes

Arwa Saud Abbas*, Hiazaa, Abdulrhman Faraj M., Abdullah Jalalah, Mohammed Alkhamisah, Rasheed Alrasheed, Fadhl S. Alfadhl, Ghadeer H. Aljalham, Fatimah Basem
King Abdulaziz City for Science and Technology (KACST), Riyadh, Saudi Arabia

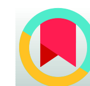

*Corresponding Author email: asabbas@kacst.edu.sa

Received: 24 August 2023 / Revised: 14 September 2023 / Accepted: 15 September 2023 / Published: 18 September 2023

ABSTRACT

The present research addresses the synthesis of carbon materials thin films by RF-PECVD in N_2/CH_4 gas mixture. Carbon materials film was formed at 40/48 sccm of CH_4/N_2 of the total gas flow rate ratio $CH_4/CH_4+N_2 = 0.45$ and 200/100 W HF/LF power at a deposition temperature of 350 °C and 1000 mTorr pressure. Then, post-annealing of carbon materials film took place at 400 °C by means of RTA under N_2 flow. The formation of carbon nanostructures was investigated by scanning electron microscopy, energy dispersive X-ray, Raman spectroscopy, and atomic force microscopy, respectively. AFM shows that the films consisted of nanocrystalline grains. The surface morphology and structural characteristics of materials were studied as a gas flow function and substrate temperature. EDX results indicated the carbon presence, and Raman spectroscopy analysis revealed two broad bands: D-band 1381.64 cm^{-1} and G-band 1589.42 cm^{-1}. The temperature-dependent post-annealing of carbon materials plays a key role in the graphite crystallites growth at high substrate temperatures. Our results indicate carbon materials incorporation for laser diode applications.

Keywords: Carbon materials, Transparent conducting oxide of tin-doped In_2O_3, Wide bandgap semiconductor.

1 Introduction

Diamond-like carbon (DLC) has a carbon-based amorphous (non-crystalline) structure. DLC has both diamond (sp^3-bonded carbon formations) and graphite (sp^2-bonded carbon formations), as shown in Figure 1 [1].

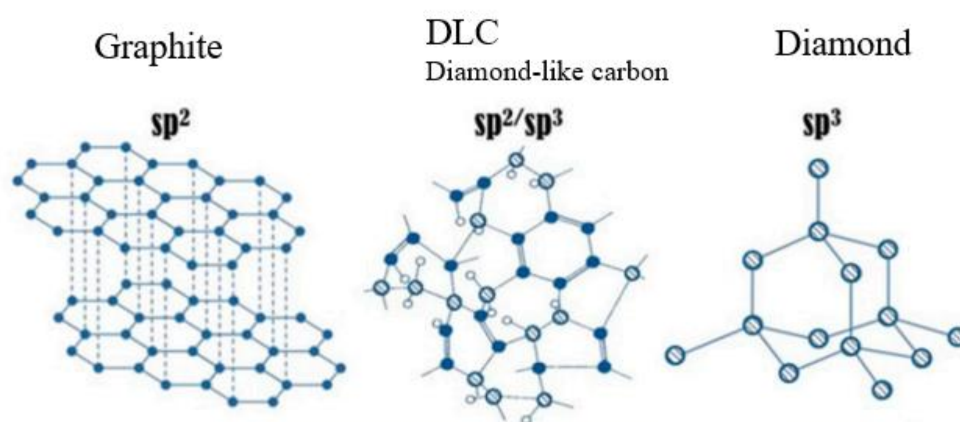

Figure 1: *Hybridizations of carbon in diamond-like carbon (DLC) films. DLC is the combination of sp^2 and sp^3. (Reproduced with permission from MDPI* [1]*).*

Copyright © 2023. The Author(s). Published by AIJR Publisher.
This is an open access article under Creative Commons Attribution-NonCommercial 4.0 International (CC BY-NC 4.0) license, which permits any non-commercial use, distribution, adaptation, and reproduction in any medium, as long as the original work is properly cited.

The DLC physical properties are defined by the ratio between sp^3 and sp^2, the hydrogen content percentage within the structure, and other metallic elements and their percentages within the material [2]. Figure 2 shows the carbon material ternary phase diagram by C. Ferrari and J. Robertson to explain the conceptual structure of DLCs [2]–[4]. The production of a-C:H DLC film is by a hydrocarbon gas, such as methane (CH_4) and acetylene (C_2H_2), using plasma enhanced chemical vapor deposition (PECVD). Hydrogenated DLCs can be classified as hydrogenated tetrahedral amorphous carbon (ta-C:H) and hydrogenated amorphous carbon (a-C:H) [2], [3]. When solid graphite and hydrocarbon gas are used as the materials to produce an a-C:H DLC [2], [3]. Carbon-based materials are required for light emitters as the band gap dependence is on the type of carbon bond.

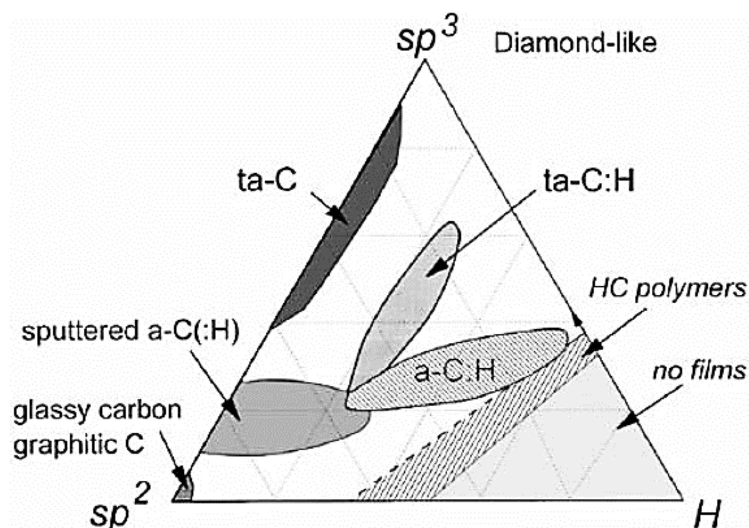

Figure 2: *Characteristic diagram of a DLC. (Reproduced with permission from Elsevier* [4]*).*

Besides, the optoelectronic devices have been confirmed to incorporate CMs with remarkable performance [5], [6]. However, CM still suffers from major obstacles regarding the absence of a convincing n-type dopant [6]. This obstacle can be overcome by simplified proposed growth techniques. CM has remained a largely unexplored material as a competitor for wide-bandgap materials. CM can be produced with different types such as diamond, graphite, DLC, and PLC [7], [8]. Z. Zheng et al. reported that CM demonstrates a wide band gap scale which depends on the hydrogen concentration and sp^3 % [7]. Diamond is an attractive material for effective UV photodetectors because its band gap, 5.47 eV at 227 nm, is equal to the energy of ultraviolet photons [7].

On the other hand, indium tin oxide (ITO) is an n-type degenerate tin-doped In_2O_3 broad, and oxygen vacancy and substitutional tin are what start the degeneracy [9]. Tin also performs as a cationic dopant in the In_2O_3 lattice and as a replacement on the indium sites to bind with the interstitial oxygen since ITO is an n-type transparent conducting oxide material [9]. Edge-emitting lasers [10]–[12] and vertical-cavity surface-emitting lasers [13] are examples of the optoelectronic devices that use ITO because of its superior optical transparency, electrical conductivity, and large band gap (>3.5 eV). Magnetron sputtering, [14]–[18] thermal evaporation, [19] pulsed laser deposition, [20], [21] and Ion beam-assisted e-beam deposition (IBAED), [9], [22], [23] are the methods commonly used to fabricate ITO thin films. Due to its low resistance, high transmittance in the visible and near infrared spectrum, stable physical and chemical properties, and strong adherence to a variety of substrates, ITO material has several of benefits [9], [24].

The implementation of the optimized ITO films onto advanced laser design has been demonstrated in InGaN based laser structure [20], [21] incorporating TCO with the thin p-GaN top cladding layers [10], [11]. However, a high substrate temperature ($\geq$ 250 °C) and an ideal oxygen flow are needed to produce ITO films with low resistance and high transmittance. ITO and CM technology has already been implemented for electrodes and current-spreading layers. Another potential technique for a transparent and

Abbas *et al.*, *Adv. Nan. Res.;* Vol. 6, Issue 1, pp: 29-43, 2023

conducting substrate is to employ ITO or CM-deposited layers over a large surface area for wide bandgap manufacturing. Jun Hee Choi et al. reported using a transparent conducting layer to enable electrical conductivity on non-conductive substrates [25], [26]. However, it is crucial fabricating simultaneous conductivity and transparency CM films at the upper of non-conductive substrates. Here, this study represents CM films deposited by PECVD onto silicon substrate at 350 °C deposition temperature and 400 °C post-annealing by means of PECVD and rapid thermal annealing (RTA) as a post-treatment method, respectively. The CM films can be tuned with annealing time under N_2 gas flow to enhance film quality. On the other hand, ITO films were deposited onto silicon substrates using the IBAED process at 250 °C with a variable oxygen flow. This research focused on the fabrication of ITO and CM films. The implementation of the paper's achievements is in line with the key guidelines for the development of lasers. In selecting the amorphous glass growth substrates which are less costly, a technique design that offers such as conductivity at the upper of non-conductive substrates is required [25], [26]. The III-nitride-based devices with mass-production are grown on sapphire substrate. Alternatively, there is potential in using conductive ITO and CM films on amorphous glass substrates or silicon substrates and as III-nitride growth substrates.

In view of light emitters, the deuterium lamp is an ultraviolet light source. Deuterium lamps emit UV light with low efficiency and low brightness [27]. On a wider scope, deuterium lamps (D_2 or ^2H – heavy hydrogen) are light sources that use an arc discharge in low pressure deuterium gas. They are considered a conventional ultraviolet light source; [27] however, a carbon-based UV light-emitting device is proposed as an alternative emitter [28]. The properties of prepared ITO and CM films were investigated by SEM, EDX, RS, Hall-effect measurements, and AFM. The results of this investigation indicate CM incorporation for laser diode applications. In addition, ITO and CM are integrated into a single device for enhancing the lifetime and efficiency of optoelectronic devices.

2 Experimental

A systematic study is performed to determine the deposition of CM using CH_4/N_2 and enhance the film adhesion with the diluted hydrogen fluoride solution. A CVD system was used for the growth of CM. The process parameters such as reacting gases and power can be selected for deposition of CM films in the chemical process. The optimized conditions were explored of the main parameters in CM synthesis of substrate temperature, gas pressure, gas mixture, and HF/LF power on silicon substrates. The growth of CM films is carried out in RF-PECVD reactor, Oxford Instruments Plasma Technology (OIPT), and PlasmaPro®100 system. Figure 3 (a) displays the CM deposition setup. Gas mixture is composed by N_2 and CH_4. Figure 3 (b) shows the steps of the PECVD recipe. CM films are grown in CH_4 with N_2 as n-type dopant [29], [30]. Films are initially deposited on Si (100) substrates that have a thickness of 500 ±50 μm, 1-side polished, p-type (boron). The area is 12x12 mm^2. Before deposition, the substrates cleaning was conducted with diluted hydrogen fluoride solution and deionized water, 1:1 DI water: HF at RT for 30 sec to remove native oxide layer and promote adhesion. The base pressure is below 4.0×10^{-2} Torr controlled by a turbo pump. PECVD substrate electrode is connected with an RF (13.56 MHz) generator.

CH_4 (99.995%) was employed for carbon-based films fabrication. The CH_4 and N_2 flow rate was at 40 and 48 sccm, respectively. The deposition temperature is 350 °C, and the pressure is 1000 mTorr for 30 min. HF/LF 200/100 W RF power and ~30 ±10 nm thickness were optimized. Following the deposition, the post-annealing of CM films was conducted by rapid thermal processor (RTP) AS-One 150-ANNEALSYS RTP system with heat lamps on top of the chamber. The substrate conditions selected the optimal temperature of 400 °C under 1000 sccm N_2 flow at a pressure of 0.1 MP for 30 min. Selecting a total temperature CM film annealing value of 750 °C and a two-step annealing of 350 °C during deposition and 400 °C using RTA resulted in a two-step change in the film properties.

ISSN: 2581-5164
Available online at Journals.aijr.org

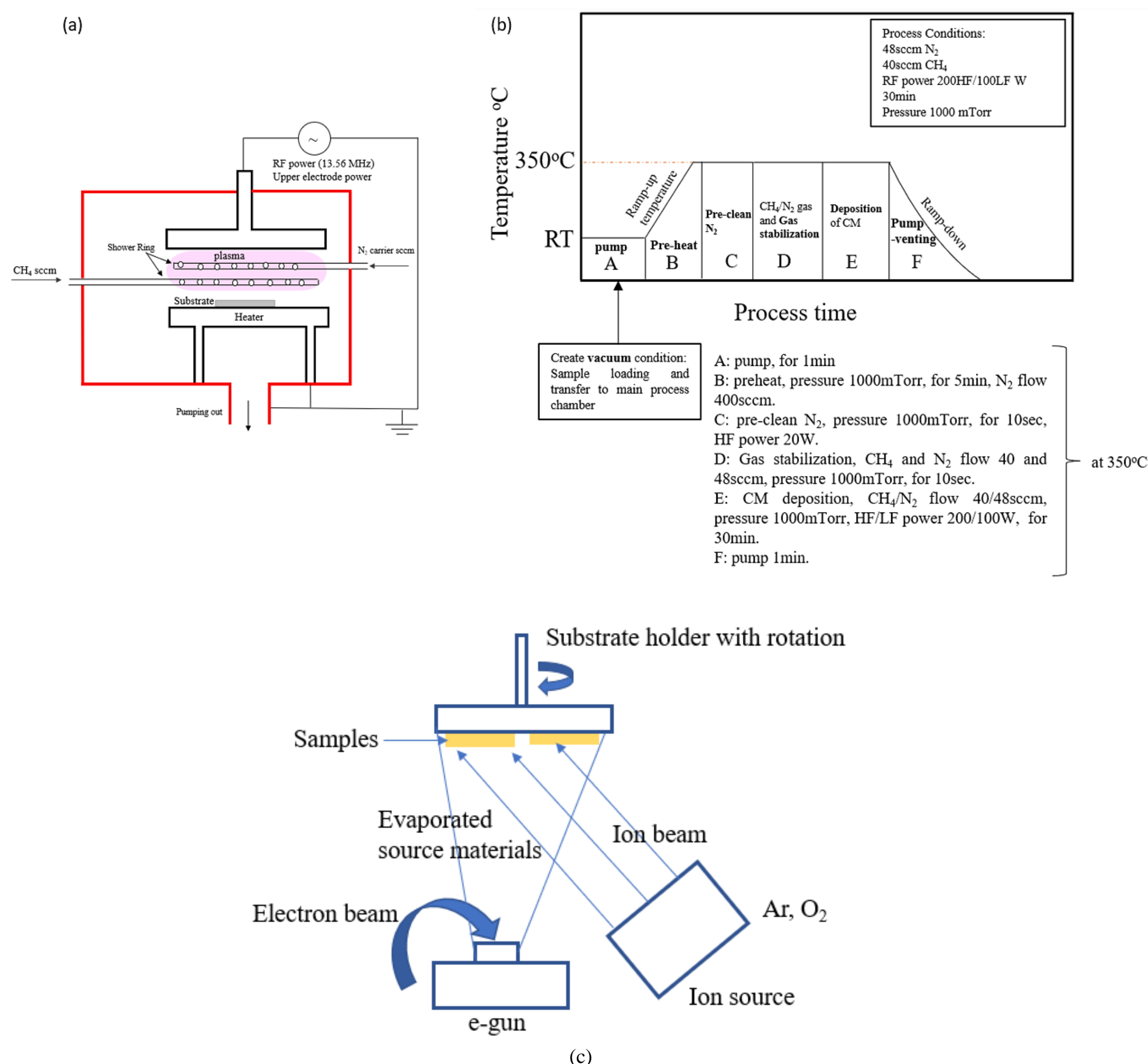

Figure 3: (a). *The CM films deposition RF-PECVD setup,* **(b).** *Process time and recipe steps, and* **(c).** *Schematic representation of IBAED deposition method apparatus*

Figure 4 (a) shows a schematic diagram of the first temperature setting introduced during PECVD deposition. Figure 4 (b) shows a recipe of RTA, post-annealing conditions; and Figure 4 (c) shows the second annealing temperature setting introduced during post-annealing. The annealing conditions were set to the following steps: A: substrate-in and temperature stabilization, B: ramp-up rate at 2 °C/sec for < 10 min (including temperature pre-stabilization), C: annealing process, and D: ramp-down 1 °C/sec for 10 min to 70 °C and substrate-out (before opening the chamber, the temperature should be less than 100 °C). The full process was ~ 50 min. However, the temperature was ramped up at 1 and 2 °C/sec and held at the selected temperatures for 30 min before ramping down at 2 and 1 °C/sec. During the cool-down, the substrate temperature must be brought down slowly to prevent dislocation and breakage of films/substrates due to thermal shock.

On the other hand, ITO films were conducted using IBAED Denton vacuum deposition systems. Figure 3 (c) shows the schematic of IBAED deposition method applied to process different oxygen flows of 10, 20, 40, 49.5 sccm onto silicon (Si) p-type (boron). Indium tin oxide (In_2O_3/SnO_2) pellets, Sn-doped with the composition of 90 wt.% In_2O_3 and 10 wt.% SnO_2 (purity of 99.99%) was conducted using IBAED. The argon ions were directed onto the substrates as extracted from a separated ion source. ITO films were deposited at a temperature of 250 °C to promote the formation of ITO grains with a roughness of < 1 nm RMS for the necessary properties, such as conductivity [13].

For the deposition of ITO at 250 °C, Nam et al. proposed transforming the amorphous state into the polycrystalline with the high annealing temperatures [13], [31]. The deposition of the large ITO grains is enhanced at a higher temperature (≥ 250 °C) [13]. Moreover, the deposition of the large ITO grains that have a value of 0.5-6 nm RMS and the resistivity (10^{-3}-10^{-4} Ω-cm) is at a higher temperature (≥ 250 °C). ITO evaporated at a rate of 0.2 nm/s. In these studies, the overall film thickness of the deposited ITO films, as determined by a step profilometer, was 150±20 nm. A step profilometer and SEM were used to measure the total film thickness, which was 150±20 nm. Cleaning the substrates was done using acetone, isopropanol, deionized water, and nitrogen flow. The chamber was evacuated prior to the deposition in order to achieve the base pressure of 9.30E-6 and 5.0E-5 mBar. Following that, an O_2 flow was conducted and set at 49.5 sccm. The deposition condition of the ion beam current accelerating voltage were 39-29 mA and 9.8 kV, respectively.

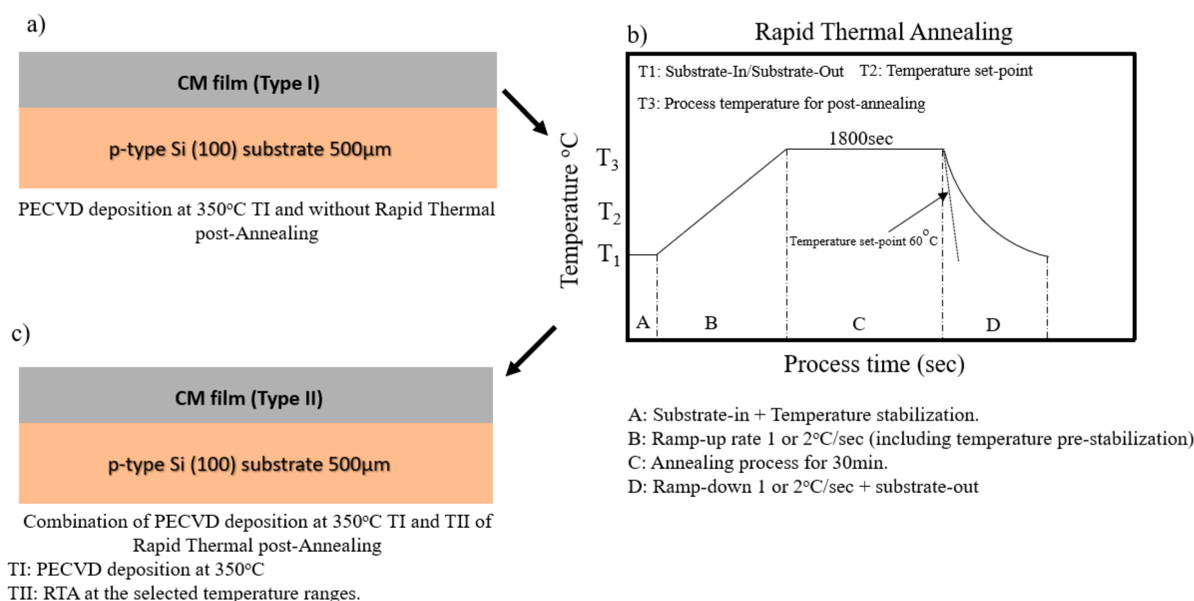

Figure 4: (a). *Schematic diagram showing the first temperature setting introduced during PECVD deposition,* **(b).** *Recipe of RTA, post-annealing conditions, and* **(c).** *The second annealing temperature setting introduced during post-annealing*

Characterization of CM deposition films by PECVD was executed by scanning electron microscope (SEM - JSM-IT300-JEOL, Japan) at an accelerating voltage of 15 kV to analyze the general morphology of the films, and this system was equipped with an EDX analyzer. The Raman spectra (RS) was carried out using confocal imaging RS (RENISHAW inVia) at 532 nm excitation laser [1]. Atomic force microscopy (AFM) was used to examine the surface morphology of the CM film. ScanAsystTM Bruker multimode scanning probe was used for AFM to analyze the surface morphology. With the ScanAsyst mode in Air, Peak Force tapping was employed at ~2 kHz drive frequency. AFM measurements are carried out in an area of 1x1 µm². Hall measurements of CM films were taken to measure the n-type conductivity with low electrical resistivity. The electrical and structural properties were conducted using Hall-effect measurements and X-ray diffraction (XRD).

3 Results and Discussion

3.1 SEM and Energy Dispersive X-ray Analysis

This system is comprised of bi-use SEM imaging and inspection as well as EDX elemental analysis. The deposited films of CMs samples were obtained by thermionic emission-scanning electron microscopy operating at 10 kV and 15 kV of acceleration voltage for top views of CM and ITO films and ITO film cross-section view, respectively. Figure 5 shows smooth surfaces of deposited films with no features.

Structural characterizations using electron microscopy reveal CM films' surface without flake-like carbon-based materials. EDX was used to find the carbon concentration in the CM films.

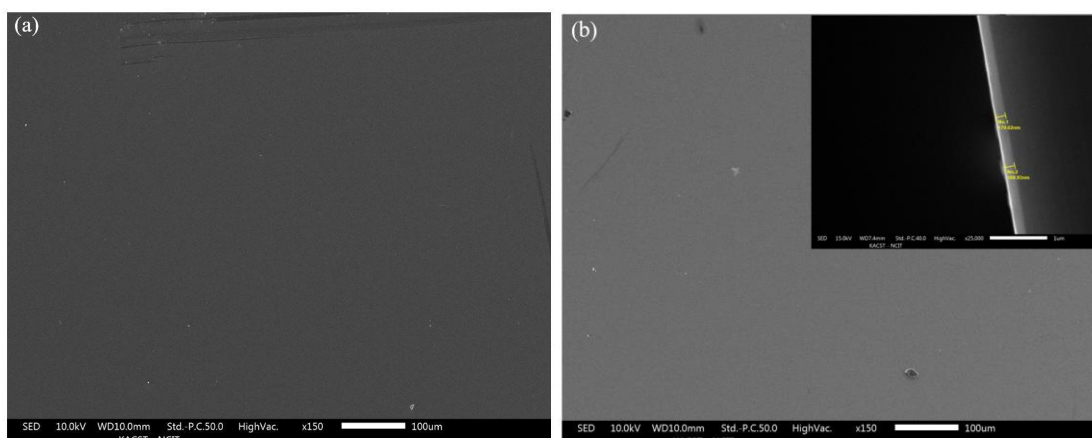

Figure 5: *SEM images: top views of* **(a).** *CM, and* **(b).** *ITO films and Inset: ITO film cross-section view*

Figure 6 shows EDX results of (a) bare silicon substrate (c) confirming the presence of carbon percentages in the films I) before and II) after post-annealing which are 2.43 wt.% (±0.98%) and 18.32 wt.% (±1.05%), respectively. This finding is similar to previously reported results, [32] where the structural evolution and resultant properties change upon heating. Also, EDX results clearly indicate ITO deposition at oxygen flow of 49.5 sccm and the presence of In: 59.45 wt.% (±1.10%), Sn: 5.85 wt.% (±1.31%), and O: 15.85 wt.% (±0.63%) as shown in Figure 6 (b).

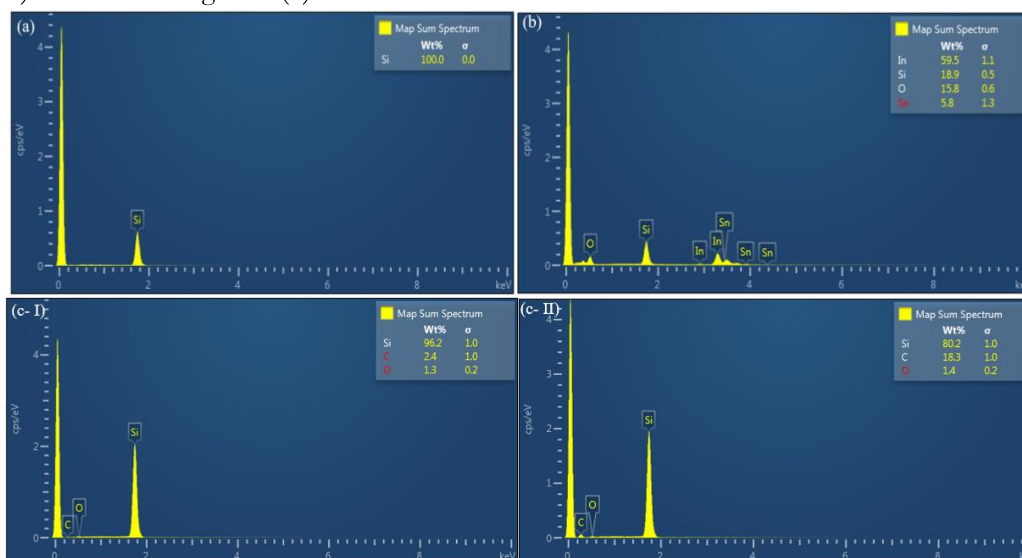

Figure 6: *EDX spectrum of* **(a).** *Bare silicon substrate,* **(b).** *ITO at 49.5 sccm oxygen flow and* **(c). I).** *Before RTA, and* **II).** *After RTA*

3.2 Raman Spectroscopy

The study of materials structural characteristics at atomic scale by measuring the photons light-scattering is conducted using RS. Unstrained silicon holds an equal frequency at 520.5 nm for the three degenerated Raman modes [33]. The polarization dependent is considered for the two transverse optical modes and one longitudinal mode, [34], [35] and the shift in frequency and intensity of three optical modes is by applied strain [36]. CM film samples are characterized applying reflection geometry by confocal imaging RS (Renishaw inVia) [1], with charge-coupled device detector of two detectors: silicon detector (300 nm–1100 nm) and InGaAs detector (1000 nm–1600 nm). The different gratings for the spectral resolution

control with 1200, 1800 and 2400 lines/mm are accessible for this work's sample setting with 2400 lines/mm grating.

The laser line of 532 nm is employed, the laser power percentage / % 0.5 that will be used for the scan and spot size of ≈1 µm at objectives 100X to modify the system spatial resolution and to confirm CM film emission [37]. Figure 7 (a) shows the Raman spectra (normalized) after applying the post-annealing of the selected temperature of 400 °C. Figure 7 (b) shows that before annealing, an increased linear spectrum without peaks was observed. With the accumulation of the presence of CMs, peaks were observed.

Moreover, the results of the Raman spectrum of CM film samples show peaks of 520.568 cm^{-1} near 960 cm^{-1}, 1381.64 nm^{-1}, and 1589.42 nm^{-1}. The second-order excitation of a Si phonon is for the peak near 960 nm^{-1}, and the 1381.64 and 1589.42 cm^{-1} peaks are sp^2-bonded carbon [2] disordered graphite. The broad overlapping peaks spectra of the G and D bands are typically observed for CM films [3]. Measuring any structural changes of thermally annealed CM films surface is indicated by Raman mode intensity. There is a carbon-rich thin film with C=C double bonds stretching at 1635 cm^{-1} [38]. Finally, the discussion of the observed transition to CM films with two peaks indicates the peaks are observed at the annealing temperature of 400 °C.

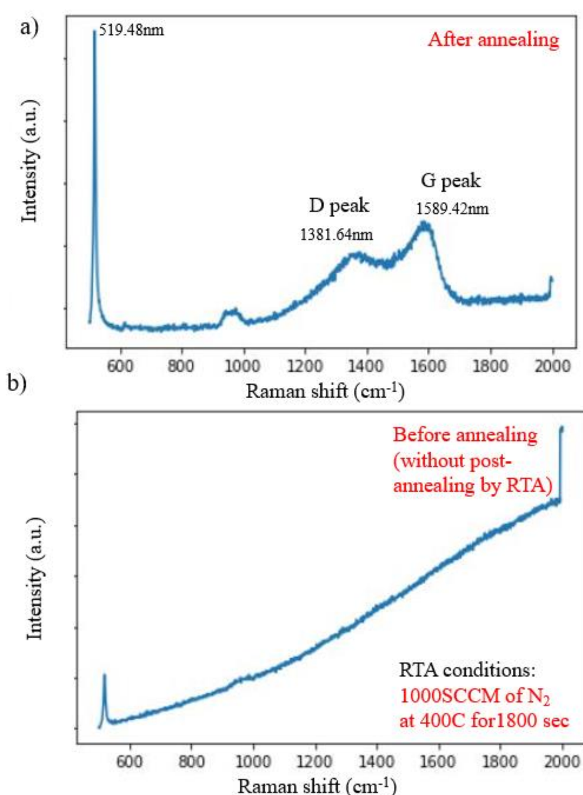

Figure 7: *Raman spectra of nitrogen-doped CM films* **a).** *with annealing,* **b).** *without annealing*

3.3 Surface Morphology

Scanning the surface of CM and ITO samples applies AFM with a sharp probe. The peak force tapping ScanAsyst is based on an imaging mode and confirms high-resolution measurements while avoiding the thin films damage. Figure 8 shows AFM images of (a) silicon substrate on CM films deposited by PECVD at 350 °C, (b) no post-annealing, and (c) at 400 °C. The roughness was abruptly enhanced with the increasing substrate temperature to 400 °C. With temperature increment to 400 °C, RMS changes from 0.581 nm to 0.476 nm. DLC is an amorphous CM films or graphite, and CVD diamond films [4].

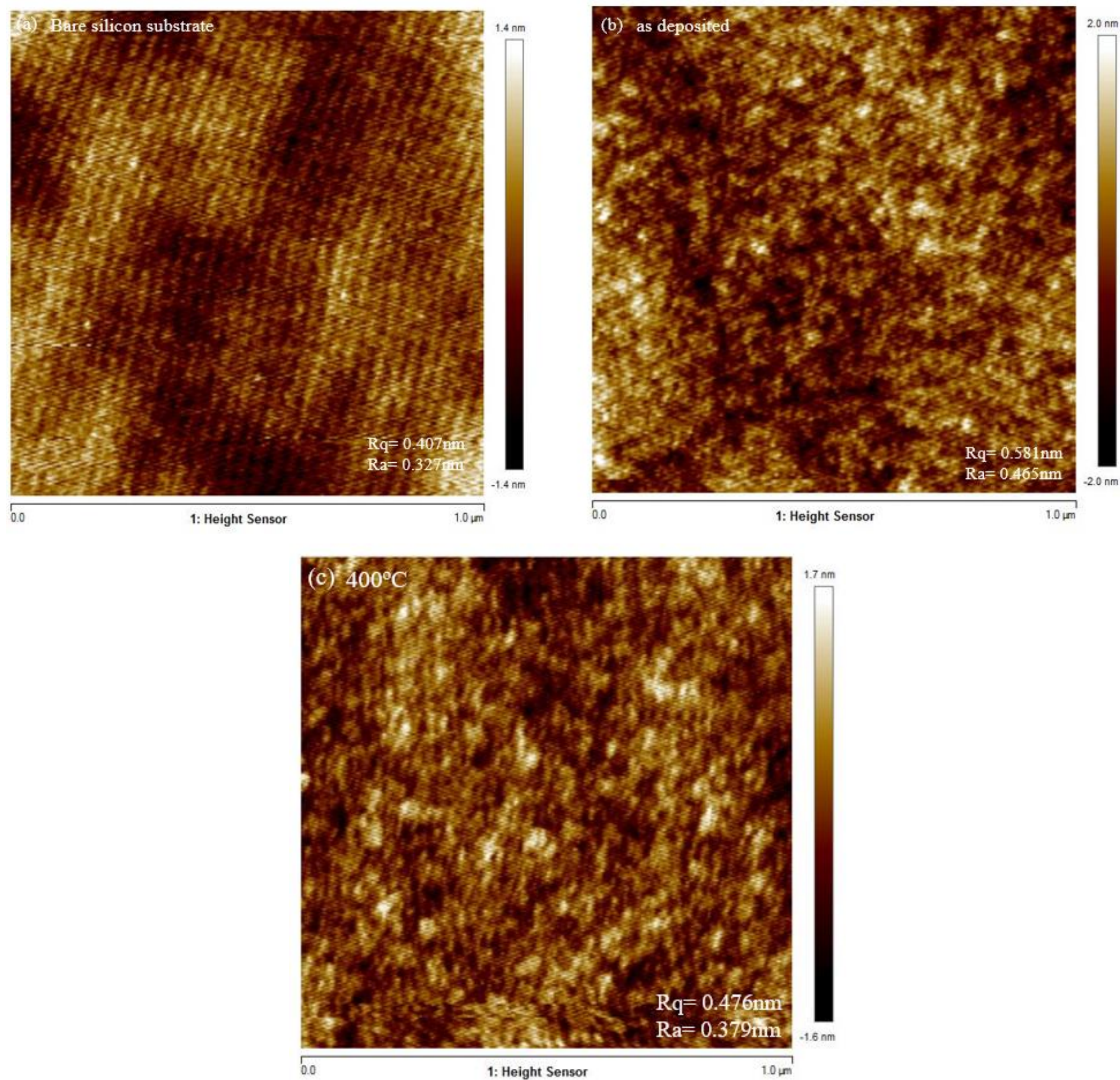

Figure 8: *AFM images of* **(a).** *Silicon substrate on CM films deposited by PECVD at 350 ^oC,* **(b).** *No post-annealing, and* **(c).** *At 400 ^oC*

As demonstrated in Figure 9, ITO films with an RMS roughness of 0.5–6 nm benefited from ITO deposition at 250 °C and oxygen flow rates of 10, 20, 30, 40, and 49.5 sccm. The annealing ITO results in a rough surface with large grain size. The quality of the deposited ITO is fabricated for an easier fit as an electrode or by being coated on the growth substrates. This study results corresponds to previous finding and following the e-beam ITO deposition parameters analysis for achieving films with <1 nm RMS and appropriate such as conductivity [39]–[42].

Abbas *et al.*, *Adv. Nan. Res.;* Vol. 6, Issue 1, pp: 29-43, 2023

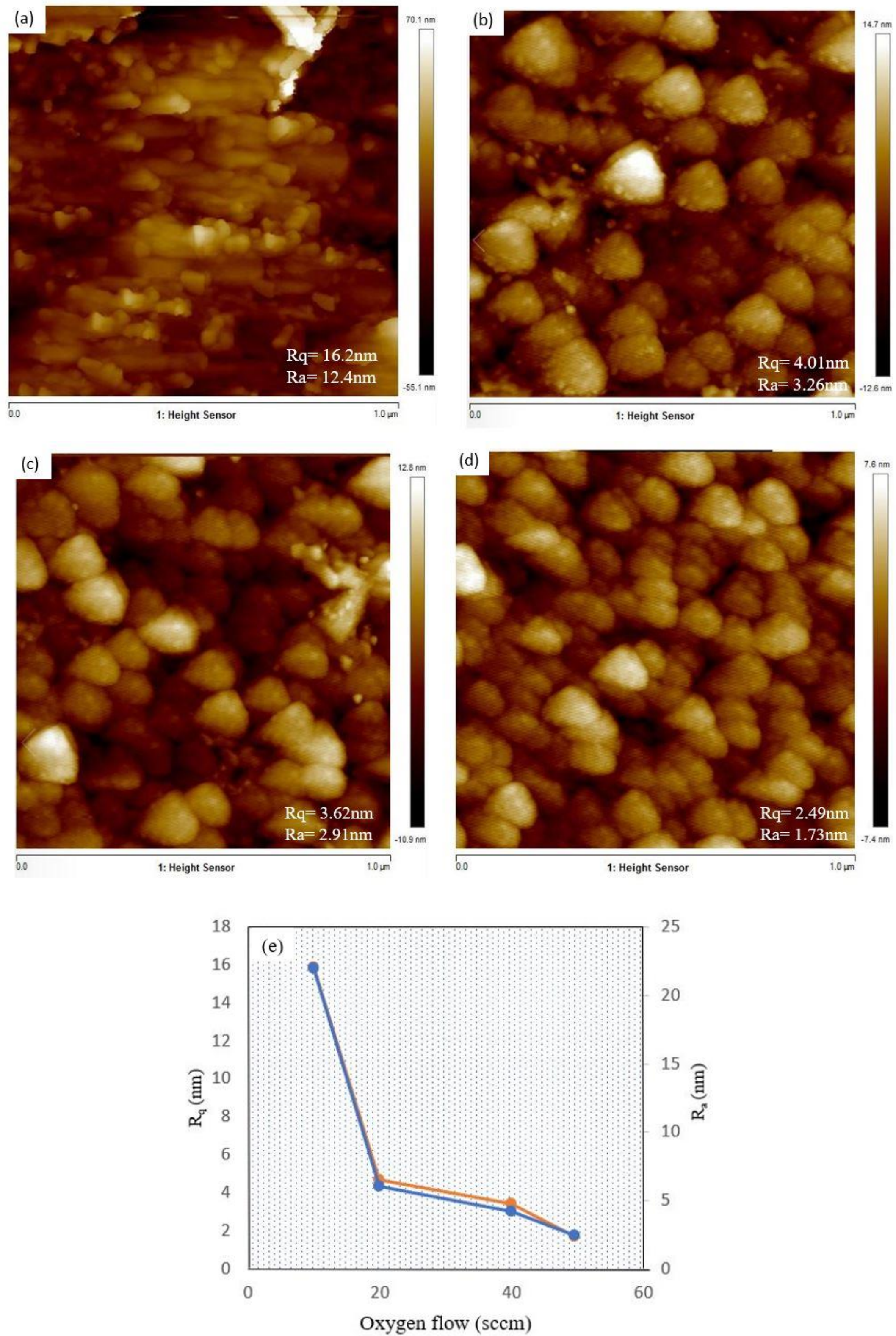

Figure 9: *AFM analysis of ITO by IBAD at 250 ºC, and the oxygen flow rate:* **(a).** *10 sccm*, **(b).** *20 sccm*, **(c).** *40 sccm*, **(d).** *49.5 sccm, and* **(e).** *RMS roughness vs. oxygen flow*

3.4 XRD Studies

The phase composition of the layers was investigated using Thermo Scientific™ ARL™ EQUINOX 1000 XRD analyzer with a Cuα radiation source over a 2θ range from 10 to 100, 40 kV, 30.6 mA, and scanning velocity of 3°/min for a total scanning time of one hour. The XRD spectra of ITO on silicon substrate are presented in Figure 10, which shows results such as (222) and (400) with a strong grain orientation in the (400) plane, thus confirming the presence of ITO. The (222) plane is the ITO films preferential growth, which is deposition conditions orientation dependent [43]. ITO films, however, crystallize in a cubic bixbyite structure (In_2O_3) after becoming polycrystalline with deposition at a high temperature, according to XRD analysis [43], [44].

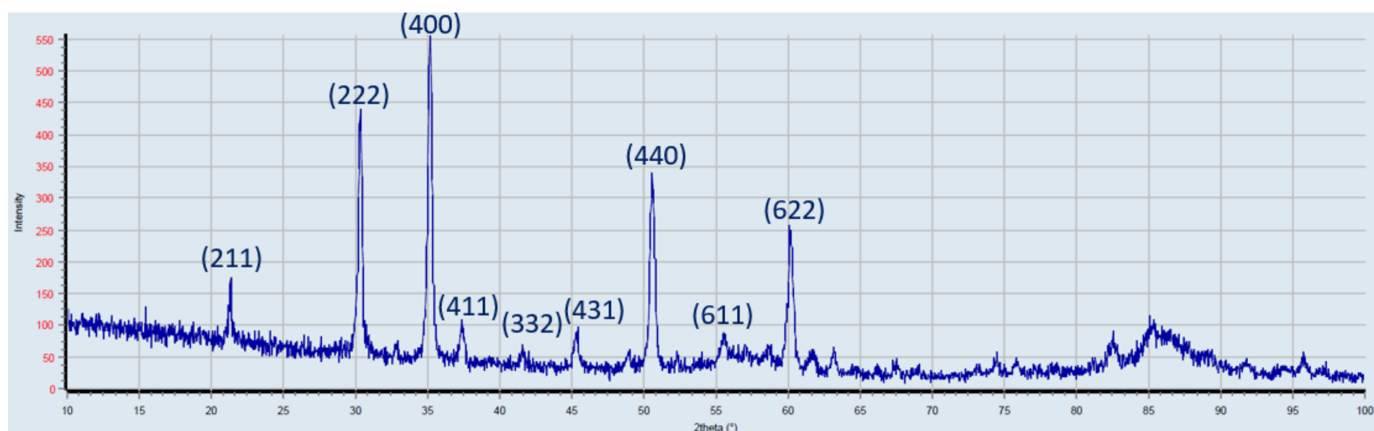

Figure 10: *XRD patterns of ITO onto silicon substrate at 250 °C and 40 sccm O_2 flow*

The detection of ITO (222), (400), (440), and (622) diffraction peaks are shown in Figure 10. At the initial deposition stage, the (222) diffraction peak is dominant. This is as a result of ITO deposition nucleation stage; indium is aggregate to densely packed (111) plane which is close to (222) diffraction peak [45]. This result is similar to research findings where the shift from (222) to (400) at a high substrate temperature due to the film thickness increasing alongside the power value [45].

3.5 Electrical Measurement using the Hall Effect

CM and ITO films have a unique property of electrical conduction towards implementations such as lasers. The optimized ITO or CM conductive films have the potential to enhance the electrical qualities. The Hall effect is used to analyze the ITO and CM films at room temperature in order to examine into the RT Hall mobility and carrier concentration. A magnetic field B deflects the electron flow (A) to one of the electrodes, and as a result of the excessive concentration of electrons close to one electrode, a resulting Hall voltage (V) can be measured [46], [47]. A magnetic field B bounces the current flow (A) to one of the electrodes and results in the excess concentration adjacent to one electrode, allowing the Hall voltage (V) to be calculated. The ITO and CM films are analyzed at RT using the Hall effect to investigate the RT Hall mobility and carrier concentration [46], [47]. The system was done according to the electrical circuit in Figure 11 [48].

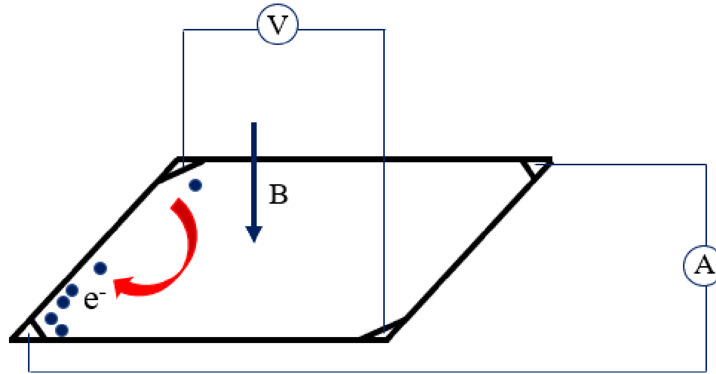

Figure 11: *Circuit diagram for Hall measurement*

The Hall coefficient: $R_H = \frac{V_H}{I} \cdot \frac{t}{B}$ (1)

The Hall coefficient R_H type defines by the sign:

$$R_H = \frac{-1}{n \cdot q} \text{ for n-type} \quad (2)$$

$$R_H = \frac{+1}{p \cdot q} \text{ for p-type} \quad (3)$$

Hall mobility μ_H:

$$\mu_H = \sigma \, |R_H| \quad (4)$$

The drift velocity calculated from:

$$v_d = \mu_H \, E_n \quad (5)$$

E_n is the applied electric field.

In this study, Hall effect system (ECOPIA-HMS-3000 VER 3.52) [46], [47] is used in a van der Pauw configuration with RT-operated electro-magnets, and magnetic flux density 0.54 T. However, the system was calibrated with standard ITO films as a reference in Table 1: T = 300 K, B = 0.53 T (field strength in tesla), and I = 5.00 mA. The deposited ITO and CM films on Si substrates are measured to obtain such as the carrier concentration, mobility, carrier type and carrier concentration.

Table 1: *The electronic properties (mobility, conductivity, carrier concentration, and resistivity) with constant current source and permanent magnets of ITO film as a standard reference by ECOPIA corporation*

ITO Sample	t= 100 nm
Sheet Resistance R_{SH} (Ω/sq)	8.125
Resistive ρ (Ω-cm)	8.125E-5
Hall mobility μ (cm^2/vs)	36.72
Electron concentration n (cm^{-3})	-2.093E+21
Conductivity (1/Ω-cm)	1.231E+4

In Table 2: (a) ITO sheet resistance of ITO is < 15 (Ω/sq), and (b) CM film results. The carbon-based materials experienced structural change as a result of annealing which led to the higher carrier concentration value and the electrical resistivity reduction down to 4.832×10^{-5} – 2.326×10^{-5} Ω·cm. The results show that the choice of the CM films' optimal deposition conditions can present improved film crystallinity, increased carrier concentration, and enhanced electrical conductivity.

Table 2: *The electronic properties (mobility, conductivity, carrier concentration, and resistivity) with constant current source and permanent magnets of* **(a).** *an ITO film, and* **(b).** *CM film*

(a).

Samples ID	**S1: t_1= 185 nm**	**S2: t_2= 152 nm**	**S3: t_3= 171 nm**	**S4: t_4= 168 nm**
Sheet Resistance R_{SH} (Ω/sq)	1.173E+1	9.625	7.478	7.569
Resistive ρ (Ω-cm)	2.170E-4	1.463E-4	1.279E-4	1.272E-4
Hall mobility μ (cm^2/vs)	3.366E-1	6.926E-2	2.464E-1	3.951E-2
Electron concentration n (cm^{-3})	-8.544E+22	-6.161E+23	-1.981E+23	-1.242E+24
Conductivity (1/Ω-cm)	4.608E+3	6.835E+3	7.820E+3	7.864E+3

(b).

Sample ID	**t_1= 30 ± 10 nm**	**t_2= 30 ± 10 nm**
Sheet Resistance R_{SH} (Ω/sq)	13.42	13.68
Resistive ρ (Ω-cm)	4.832E-05	2.326E-05
Hall mobility μ (cm^2/vs)	27.23	28
Carrier concentration n (cm^{-3})	4.745E+21	9.584E+21
Conductivity (1/Ω-cm)	2.069E+04	4.299E+04

ITO and CM films' hall measurements revealed low electrical resistivity and n-type conductivity (2.170×10^{-4} cm and 4.832×10^{-5} cm, respectively). Importantly, modifying the annealing recipe could lead to flakes formation, [49] which is part of an advanced transfer technique for flexible light emitter devices using CMs as a hosted substrate, and transferring the grown high-quality GaN to the upper ITO and CM films. However, the ITO and CM films electrical properties are sensitive to process conditions. Thus, the deposition of ITO and CM films are at > 200 °C, to acquire a thin film with < 2×10^{-4} Ω·cm resistivity. Carbon-based semiconductor materials, with the hall mobility was > 20 cm^2/vs and carrier concentration of ~ 1021 cm^{-3} were achieved. The results indicate CM incorporation for laser diode applications [50], [51].

4 Conclusion

Carbon-based materials films deposited by RF-PECVD using CH_4 and N_2 were post-annealing at 400 °C under 1000 sccm N_2 flow using rapid thermal annealing (RTA). Graphitic carbon was obtained according to this study's findings. The crystallization conversion is found to be strongly dependent on the annealing

processes. The results show that the choice of the CM films' optimal deposition conditions can present improved film crystallinity, increased carrier concentration, and enhanced electrical conductivity. The findings by RS show the growth of graphite crystallites that enhanced at the elevated temperature. RS analysis revealed two broad bands: D-band 1381.64 cm^{-1} and G-band 1589.42 cm^{-1}. The temperature-dependent post-annealing of CMs plays a key role in the growth of graphite crystallites. Our results indicate CM incorporation for laser diode applications.

5 Declaration

5.1 Acknowledgment

The fund is by the King Abdulaziz City for Science and Technology (KACST) through utilizing KACST cleanroom and KACST facilities. Thanks for assistance regarding arrangement for the 1st cleanroom staff meeting and for laboratory equipment booking, Thamer A. Tabbakh; analysis for UV-Vis-NIR spectrophotometer, Faiyz H. Alotibi; thanks for ORBIT-KACST team for discussion regarding PECVD operation.

5.2 Author Contributions

Conceptualization, ARWA SAUD ABBAS (ASA); methodology and validation, ASA; investigation, ASA, writing the original draft preparation, ASA; supervision, ASA, resources, KACST cleanroom, data curation, ASA. PECVD, RTA, Filmetrics, Hiazaa, Abdulrhman Faraj M (HA), IBAD, Abdullah Jalalah (AJ); arranging the KACST cleanroom tool reservation, AH and AJ; AFM analysis, Mohammed Alkhamisah (MA); XRD analysis, Rasheed Alrasheed (RA); SEM and EDX analysis, Fadhl S. Alfadhl (FA); analysis for Raman spectroscopy with Arwa's assistance in loading and unloading samples and conditions setting and the demonstration of process flow with, Ghadeer H. Aljalham (GA) at Prof. Moh Amer laboratory; analysis for Hall measurement, Fatimah Basem (FB); ASA led the team. Authors have read and agreed to the published version of the manuscript.

5.3 Competing Interests

The authors declared that no conflict of interest exists in this work.

5.4 Publisher's Note

AIJR remains neutral with regard to jurisdiction claims in institutional affiliations.

How to Cite this Article:

A. S. Abbas, A. F. M. Hiazaa, A. Jalalah, M. Alkhamisah, R. Alrasheed, F. S. Alfadhl, G. H. Aljalham, and F. Basem, "Fabrication Method of Carbon-based Materials in CH_4/N_2 Plasma by RF-PECVD and Annealing Treatment for Laser Diodes", *Adv. Nan. Res.*, vol. 6, no. 1, pp. 29–43, Sep. 2023. https://doi.org/10.21467/anr.6.1.29-43

References

[1] S. N. Grigoriev, M. A. Volosova, S. V. Fedorov, and M. Mosyanov, "Influence of DLC Coatings Deposited by PECVD Technology on the Wear Resistance of Carbide End Mills and Surface Roughness of AlCuMg2 and 41Cr4 Workpieces," *Coatings*, vol. 10, no. 11, p. 1038, Oct. 2020.

[2] Y. Tanaka, K. Miyake, and A. Saito, "Diamond-like carbon film for bearing parts and its mass production technology," *SEI Technical Review*, no. 88, 2019.

[3] C. Casiraghi, J. Robertson, and A. C. Ferrari, "Diamond-like carbon for data and beer storage," *Materials Today*, vol. 10, no. 1–2. 2007. doi: 10.1016/S1369-7021(06)71791-6.

[4] J. Robertson, "Diamond-like amorphous carbon," *Materials Science and Engineering: R: Reports*, vol. 37, no. 4–6, pp. 129–281, May 2002.

[5] J. Y. Tsao *et al.*, "Ultrawide-Bandgap Semiconductors: Research Opportunities and Challenges," *Advanced Electronic Materials*, vol. 4, no. 1. 2018. doi: 10.1002/aelm.201600501.

[6] C. J. H. Wort and R. S. Balmer, "Diamond as an electronic material," *Materials Today*, vol. 11, no. 1–2. 2008. doi: 10.1016/S1369-7021(07)70349-8.

[7] Z. Zheng, "Diamond-Like Carbon Films Made by Sputtering and PECVD," 1997.

[8] A. S. Tremsin and O. H. W. Siegmund, “UV photoemission efficiency of polycrystalline CVD diamond films,” *Diam Relat Mater*, vol. 14, no. 1, 2005, doi: 10.1016/j.diamond.2004.06.039.

[9] L. J. Meng, E. Liang, J. Gao, V. Teixeira, and M. P. D. Santos, “Study of indium tin oxide thin films deposited on acrylics substrates by ion beam assisted deposition technique,” in *Journal of Nanoscience and Nanotechnology*, 2009. doi: 10.1166/jnn.2009.M24.

[10] A. Myzaferi *et al.*, “Transparent conducting oxide clad limited area epitaxy semipolar III-nitride laser diodes,” *Appl Phys Lett*, vol. 109, no. 6, 2016, doi: 10.1063/1.4960791.

[11] A. Myzaferi, A. H. Reading, R. M. Farrell, D. A. Cohen, S. Nakamura, and S. P. DenBaars, “Semipolar III-nitride laser diodes with zinc oxide cladding,” *Opt Express*, vol. 25, no. 15, 2017, doi: 10.1364/oe.25.016922.

[12] S. Mehari, D. A. Cohen, D. L. Becerra, S. Nakamura, and S. P. DenBaars, “Demonstration of enhanced continuous-wave operation of blue laser diodes on a semipolar 202¯1¯ GaN substrate using indium-tin-oxide/thin-p-GaN cladding layers,” *Opt Express*, vol. 26, no. 2, 2018, doi: 10.1364/oe.26.001564.

[13] S. G. Lee *et al.*, “Continuous-wave operation of nonpolar GaN-based vertical-cavity surface-emitting lasers,” 2018. doi: 10.1117/12.2314885.

[14] J. H. Park, C. Buurma, S. Sivananthan, R. Kodama, W. Gao, and T. A. Gessert, “The effect of post-annealing on Indium Tin Oxide thin films by magnetron sputtering method,” *Appl Surf Sci*, vol. 307, 2014, doi: 10.1016/j.apsusc.2014.04.042.

[15] K. S. Tseng and Y. L. Lo, “Effect of sputtering parameters on optical and electrical properties of ITO films on PET substrates,” *Appl Surf Sci*, vol. 285, no. PARTB, 2013, doi: 10.1016/j.apsusc.2013.08.024.

[16] K. C. Heo, Y. Sohn, and J. S. Gwag, “Effects of an additional magnetic field in ITO thin film deposition by magnetron sputtering,” *Ceram Int*, vol. 41, no. 1, 2015, doi: 10.1016/j.ceramint.2014.08.111.

[17] Y. S. Jung, D. W. Lee, and D. Y. Jeon, “Influence of dc magnetron sputtering parameters on surface morphology of indium tin oxide thin films,” *Appl Surf Sci*, vol. 221, no. 1–4, 2004, doi: 10.1016/S0169-4332(03)00862-6.

[18] A. Klöppel *et al.*, “Dependence of the electrical and optical behaviour of ITO-silver-ITO multilayers on the silver properties,” *Thin Solid Films*, vol. 365, no. 1, 2000, doi: 10.1016/S0040-6090(99)00949-9.

[19] K. Y. Pan, L. Da Lin, L. W. Chang, and H. C. Shih, “Studies on the optoelectronic properties of the thermally evaporated tin-doped indium oxide nanostructures,” *Appl Surf Sci*, vol. 273, 2013, doi: 10.1016/j.apsusc.2012.12.149.

[20] J. B. Choi, J. H. Kim, K. A. Jeon, and S. Y. Lee, “Properties of ITO films on glass fabricated by pulsed laser deposition,” in *Materials Science and Engineering B: Solid-State Materials for Advanced Technology*, 2003. doi: 10.1016/S0921-5107(02)00625-6.

[21] J. M. Dekkers, G. Rijnders, and D. H. A. Blank, “Role of Sn doping in In2O3 thin films on polymer substrates by pulsed-laser deposition at room temperature,” *Appl Phys Lett*, vol. 88, no. 15, 2006, doi: 10.1063/1.2195096.

[22] Y. C. Park, Y. S. Kim, H. K. Seo, S. G. Ansari, and H. S. Shin, “ITO thin films deposited at different oxygen flow rates on Si(100) using the PEMOCVD method,” *Surf Coat Technol*, vol. 161, no. 1, 2002, doi: 10.1016/S0257-8972(02)00476-0.

[23] Y. S. Kim, Y. C. Park, S. G. Ansari, B. S. Lee, and H. S. Shin, “Effect of substrate temperature on the bonded states of indium tin oxide thin films deposited by plasma enhanced chemical vapor deposition,” *Thin Solid Films*, vol. 426, no. 1–2, 2003, doi: 10.1016/S0040-6090(03)00005-1.

[24] K. L. Chopra, S. Major, and D. K. Pandya, “Transparent conductors-A status review,” *Thin Solid Films*, vol. 102, no. 1. 1983. doi: 10.1016/0040-6090(83)90256-0.

[25] J. H. Choi *et al.*, “Nearly single-crystalline GaN light-emitting diodes on amorphous glass substrates,” *Nat Photonics*, vol. 5, no. 12, 2011, doi: 10.1038/nphoton.2011.253.

[26] J. H. Choi *et al.*, “Fully flexible gan light-emitting diodes through nanovoid-mediated transfer,” *Adv Opt Mater*, vol. 2, no. 3, 2014, doi: 10.1002/adom.201300435.

[27] Photron Pty. Ltd., “Deuterium Lamps. Photron Pty. Ltd.,” Mar. 04, 2016. https://web.archive.org/web/20160304025924/http://www.photron.com.au/.assets/brochures/deuterium_lamp.pdf (accessed Sep. 18, 2023).

[28] K. Meguro, K. Tanizaki, Y. Yamamoto, and T. Imai, “Diamond substrate and its manufacturing method,” JP2006273592A, Mar. 28, 2005

[29] S. C. Eaton, A. B. Anderson, J. C. Angus, Y. E. Evstefeeva, and Y. V. Pleskov, “Co-doping of diamond with boron and sulfur,” *Electrochemical and Solid-State Letters*, vol. 5, no. 8, 2002, doi: 10.1149/1.1486821.

[30] W. Haenni, P. Rychen, M. Fryda, and C. Comninellis, “Chapter 5 Industrial applications of diamond electrodes,” *Semiconductors and Semimetals*, vol. 77, no. C, pp. 149–196, Jan. 2004, doi: 10.1016/S0080-8784(04)80017-6.

[31] E. Nam, Y. H. Kang, D. J. Son, D. Jung, S. J. Hong, and Y. S. Kim, “Electrical and surface properties of indium tin oxide (ITO) films by pulsed DC magnetron sputtering for organic light emitting diode as anode material,” *Surf Coat Technol*, vol. 205, no. SUPPL. 1, 2010, doi: 10.1016/j.surfcoat.2010.06.060.

[32] K. Mondal, J. Kumar, and A. Sharma, “ TiO 2 -nanoparticles-impregnated photocatalytic macroporous carbon films by spin coating ,” *Nanomaterials and Energy*, vol. 2, no. 3, 2013, doi: 10.1680/nme.12.00034.

[33] Z. Iqbal and S. Veprek, “Raman scattering from hydrogenated microcrystalline and amorphous silicon,” *Journal of Physics C: Solid State Physics*, vol. 15, no. 2, 1982, doi: 10.1088/0022-3719/15/2/019.

[34] E. Anastassakis, A. Pinczuk, E. Burstein, F. H. Pollak, and M. Cardona, “Effect of static uniaxial stress on the Raman spectrum of silicon,” *Solid State Commun*, vol. 8, no. 2, 1970, doi: 10.1016/0038-1098(70)90588-0.

[35] M. Becker, H. Scheel, S. Christiansen, and H. P. Strunk, “Grain orientation, texture, and internal stress optically evaluated by micro-Raman spectroscopy,” *J Appl Phys*, vol. 101, no. 6, 2007, doi: 10.1063/1.2434961.

[36] M. De Biasio *et al.*, “Determination of stress in silicon wafers using Raman spectroscopy,” in *Next-Generation Spectroscopic Technologies VIII*, 2015. doi: 10.1117/12.2176994.

[37] “TM002-02-A Introduction to WiRE and System start-up,” *Cornell Center for Materials Research*, Aug. 2016. https://www.ccmr.cornell.edu/wp-content/uploads/sites/2/2016/08/Wire4_Training_Modules_Compilation-Part-2.pdf (accessed Sep. 15, 2023).

[38] K. J. Cho *et al.*, "Fabrication and characteristics of amorphous carbon films grown in pure methane plasma by using radio frequency plasma enhanced chemical vapor deposition," *Japanese Journal of Applied Physics, Part 1: Regular Papers and Short Notes and Review Papers*, vol. 42, no. 4 A, 2003, doi: 10.1143/jjap.42.1744.

[39] D. Raoufi, A. Kiasatpour, H. R. Fallah, and A. S. H. Rozatian, "Surface characterization and microstructure of ITO thin films at different annealing temperatures," *Appl Surf Sci*, vol. 253, no. 23, 2007, doi: 10.1016/j.apsusc.2007.05.032.

[40] D. Raoufi, "Morphological characterization of ITO thin films surfaces," *Appl Surf Sci*, vol. 255, no. 6, 2009, doi: 10.1016/j.apsusc.2008.10.020.

[41] R. X. Wang, C. D. Beling, S. Fung, A. B. Djurišic, C. C. Ling, and S. Li, "Influence of gaseous annealing environment on the properties of indium-tin-oxide thin films," *J Appl Phys*, vol. 97, no. 3, 2005, doi: 10.1063/1.1834984.

[42] R. X. Wang *et al.*, "Influence of annealing temperature and environment on the properties of indium tin oxide thin films," *J Phys D Appl Phys*, vol. 38, no. 12, 2005, doi: 10.1088/0022-3727/38/12/022.

[43] H. L. Ma, D. H. Zhang, P. Ma, S. Z. Win, and S. Y. Li, "Preparation and properties of transparent conducting indium tin oxide films deposited by reactive evaporation," *Thin Solid Films*, vol. 263, no. 1, 1995, doi: 10.1016/0040-6090(95)06554-7.

[44] S. H. Brewer and S. Franzen, "Calculation of the electronic and optical properties of indium tin oxide by density functional theory," *Chem Phys*, vol. 300, no. 1–3, 2004, doi: 10.1016/j.chemphys.2003.11.039.

[45] R. Balasundaraprabhu, E. V. Monakhov, N. Muthukumarasamy, O. Nilsen, and B. G. Svensson, "Effect of heat treatment on ITO film properties and ITO/p-Si interface," *Mater Chem Phys*, vol. 114, no. 1, 2009, doi: 10.1016/j.matchemphys.2008.09.053.

[46] Bridge Technology, "Ecopia low cost Hall effect measurement system for van der pauw method," *Bridge Technology*.

[47] L. H. W. Van Beveren *et al.*, "Indium tin oxide film characterization using the classical Hall Effect," in *2014 Conference on Optoelectronic and Microelectronic Materials and Devices, COMMAD 2014*, 2014. doi: 10.1109/COMMAD.2014.7038675.

[48] O. Adnan, "Electroluminescence of white light from ZnO nanostructures/TPD hybrid," University of Baghdad, Karrada, 2015.

[49] S. Vaziri, "Fabrication and Characterization of Graphene Field Effect Transistors," *Thesis*, 2011.

[50] A. S. Abbas, "Ultrawide-bandgap semiconductor of carbon-based materials for meta-photonics-heterostructure, lasers, and holographic displays," *AAPPS Bulletin*, vol. 33, no. 1, 2023, doi: 10.1007/s43673-022-00073-0.

[51] A. Oyekunle, "Diamond Keeps Growing as a WBG Material for High-power and Frequency Electronics," *All About Circuits*, Mar. 09, 2022.

Publish your research article in AIJR journals-

- ✓ Online Submission and Tracking
- ✓ Peer-Reviewed
- ✓ Rapid decision
- ✓ Immediate Publication after acceptance
- ✓ Articles freely available online
- ✓ Retain full copyright of your article.

Submit your article at journals.aijr.org

Publish your books with AIJR publisher-

- ✓ Publish with ISBN and DOI.
- ✓ Publish Thesis/Dissertation as Monograph.
- ✓ Publish Book Monograph.
- ✓ Publish Edited Volume/ Book.
- ✓ Publish Conference Proceedings
- ✓ Retain full copyright of your books.

Submit your manuscript at books.aijr.org